Bull. Mater. Sci., Vol. 37, No. 3, May 2014, pp. 705–711. © Indian Academy of Sciences.

Structural, electrical and electrochemical behaviours of $LiNi_{0.4}M_{0.1}Mn_{1.5}O_4$ (M = Al, Bi) as cathode material for Li-ion batteries

G P NAYAKA, J MANJANNA*, K C ANJANEYA, P MANIKANDAN[†], P PERIASAMY[†] and V S TRIPATHI[††]

Department of Industrial Chemistry, Kuvempu University, Shankaraghatta 577 451, India
[†]Central Electrochemical Research Institute, Karaikudi 630 006, India
[††]Chemistry Group, Bhabha Atomic Research Centre, Mumbai 400 085, India

MS received 13 February 2013; revised 30 May 2013

Abstract. In order to improve the cycling performance of $LiMn_2O_4$ based cathode materials, we have synthesized a new composition, $LiNi_{0.4}M_{0.1}Mn_{1.5}O_4$ (M = Al, Bi), by the sol–gel method. The formation of solid solutions is confirmed by structural characterization using TG/DTA, XRD, FT–IR, EPR, SEM and EPR. A.c.-impedance (Nyquist plot) showed a high frequency semicircle and a sloping line in the low-frequency region. The semicircle is ascribed to the Li-ion migration through the interface from the surface layer of the particles to the electrolyte. Cyclic voltammogram (between 3·5 and 4·9 V) for these materials using CR2032 coin-type cell shows two pairs of redox peaks corresponding to two-step reversible intercalation process, wherein Li-ions occupy two different tetragonal 8a sites in spinel $Li_xMn_2O_4$ ($x < 1$) lattice. The galvanostatic charge/discharge curves for M = Al (77 mAh g^{-1}) showed reasonably good capacity retention than that of M = Bi (11 mAh g^{-1}) at the end of 17th cycle.

Keywords. Lithium ion batteries; $LiNi_{0.4}M_{0.1}Mn_{1.5}O_4$ (M = Al, Bi); cyclic voltammetry; a.c.-impedance; charge/discharge.

1. Introduction

Lithium ion batteries (LIB) are widely used for consumer electronic devices like cellular phones and portable computers due to their high voltage, portability and excellent cyclability (Okubo *et al* 2007) to meet certain demands of our modern society. The commercially successful LIBs make use of layered $LiCoO_2$ cathodes. Due to the high cost and toxicity of cobalt here, led to the development of cheaper and environmentally benign cathode materials. In this regard, $LiMn_2O_4$ based spinels are attractive alternatives, viz., high rate performance, high energy density, low cost, low toxicity and can be easily prepared compared to $LiCoO_2$ or Li(Co, Ni)O_2 used in commercial Li-ion cells (Kim and Manthiram 1997; Michalska *et al* 2011), although the design, integrity and cyclability is the main challenges (Poizot *et al* 2000).

$LiMn_2O_4$ has a spinel structure, space group *Fd3m*, with a cubic close packing of O^{2-} anions in which the Li^+ are in the 8(a) tetrahedral and the $Mn^{3+,4+}$ are in the 16(d) octahedral sites. The $(Mn_2)O_4$ frame work defines a three-dimensional network of channels through which Li^+ can diffuse. Although the $LiMn_2O_4$ can be cycled in the 4 V region, gradual loss of capacity on cycling is observed (Aklalouch *et al* 2009). Such a loss of capacity is due to: (i) dissolution of Mn^{2+} formed by the disproportionation reaction, $2Mn^{3+}_{(s)} \rightarrow Mn^{4+}_{(s)} + Mn^{2+}_{(soln.)}$ (Huggins 2008) by the HF acid attack, generated by hydrolysis of $LiPF_6$ electrolyte, (ii) the onset of John–Teller (J–T) distortion on the crystal structure at the end of discharge, i.e. large change in the unit cell volume due to loss of Mn^{3+} ions (Amatucci *et al* 1999) and (iii) mechanical instability due to structural changes during Li^+ de/insertion in the charge/discharge steps. It is possible that all the three phenomena contribute concurrently to the capacity fade of the $LiMn_2O_4$ electrode (Amarilla *et al* 2009). A notable improvement in the cycling performance occurs when the $LiMn_2O_4$ is doped with different metallic cations such as Ni^{2+}, Cr^{3+}, Co^{3+} and Al^{3+}. In fact, substitution for Mn^{3+} by other matals decreases the dissolution of the $LiMn_2O_4$ based spinels and suppresses the J–T effect also reduces the volume difference between the charged/discharged structures of the doped spinel (Wang *et al* 1999; Shin and Manthiram 2002, 2003). Recently, it has been demonstrated that double doping, particularly when Li^+ is one of the doping cations, improves the cycling performance of the $LiMn_2O_4$-based cathodes (Shin and Manthiram 2003). For practical applications, high rate capability is one of the most important characteristics of electrode materials (Aklalouch *et al* 2009; Amarilla *et al* 2009).

*Author for correspondence (jmanjanna@rediffmail.com)

It is in this direction that we have explored the electrochemical behaviour of Al and Bi-doped spinels, $LiNi_{0.4}M_{0.1}Mn_{1.5}O_4$ (M = Al, Bi) for Li-ion battery as cathode materials.

Furthermore, commercial $LiMn_2O_4$ powder is usually prepared by solid-state reactions, which often lead to inhomogeneties, irregular morphology and broad distribution of particle sizes. To overcome these drawbacks, many soft chemical approaches such as co-precipitation (Hassoun *et al* 2011), combustion (Amarilla *et al* 2009), microwave (Whitfield and Davidson 2000), hydrothermal (Ye *et al* 2010), sol–gel (Michalska *et al* 2011) and microemulsion (Ke *et al* 2010) methods have been developed. Hence, in the present study we have adopted a sol–gel method using citric acid followed by calcination at high temperature. Thus, we describe the structural, electrical and electrochemical behaviour of $LiNi_{0.4}M_{0.1}Mn_{1.5}O_4$ (M = Al, Bi) here.

2. Experimental

$LiNi_{0.4}M_{0.1}Mn_{1.5}O_4$ (M = Al, Bi) oxides in the powder form was prepared by taking the stoichiometric amounts of the constituent elements, viz. $LiOH{\cdot}H_2O$, $(C_2H_3O_2)_2Mn{\cdot}4H_2O$, $(C_2H_3O_2)_2Ni{\cdot}4H_2O$, $Bi(NO_3){\cdot}5H_2O$ and anhydrous $Al(OH)_3$ dissolved in deionized water with a drop of nitric acid. Citric acid monohydrate ($C_6H_8O_7{\cdot}H_2O$), a chelating agent, was added to this solution keeping a metal ion to ligand ratio of 1 : 1. The mixture was stirred vigorously at 90 °C till it formed a viscous liquid, gel. Then, it was dried at 150 °C for few hours and after grinding to fine powder in agate mortar, it was heated to 350 °C/4 h to obtain an intermediate compound followed by final calcination at 900 °C/22 h to form $LiNi_{0.4}M_{0.1}Mn_{1.5}O_4$ (M = Al, Bi).

X-ray diffraction (XRD) pattern was obtained using CuKα radiation (λ = 1·542 Å) with a Ni-filter (Bruker D8 Advance X-ray diffractometer). The scanning electron microscopy (SEM) was used to evaluate the morphology of the sample and the elemental composition by recording energy dispersive X-ray (EDX) spectra. FT–IR spectra was obtained with KBr pellet.

Electron paramagnetic resonance (EPR) studies were made by a Bruker EMX plus X-band spectrometer, with a 100 kHz field modulation operating at 9·8 GHz frequency. The microwave power level was kept at 0·6 mW. The scan range was 6000 G and the spectra were registered at room temperature.

The electrical and electrochemical studies were performed with a CR-2032 coin type cells assembled in an Ar-filled glow box. The spinel powder (80 wt%), super P carbon black (15 wt%) and a polyvinylidene fluoride (5 wt%) were ground with a drop of *N*-methylpyrrolidone solvent to form a homogeneous slurry. This slurry coated on Al-foil was dried in ambient condition and cut in to circular discs. Li-foil was used as both negative and reference electrode. The electrodes were separated by a Celgard® 2400 (polypropylene) soaked in the electrolyte, 1 M solution of $LiPF_6$ in ethylene carbonate–dimethyl carbonate (EC/DMC, 1 : 1). The components were assembled to CR-2032 coin type cells in argon filled glove box.

A.c.-impedance data was obtained using Autolab PGSTAT 302N computer-controlled potentiostat with frequency response analyser (FRA2) for CR-2032 coin type cells in the frequency range of 10 kHz–100 MHz.

A cyclic voltammogram was recorded using Autolab PGSTAT 302n for a CR-2032 coin type cells which formed a three electrode cell – the working electrode, i.e. the active cathode material was combined with a Li-foil used as reference and counter electrode. A scan rate of 0·1 mV s^{-1} between 3·5 and 4·9 V vs Li was set.

Charge–discharge cycle tests were carried out between 3·5 and 4·9 V at C/10 rate using Arbin battery system.

3. Results and discussion

3.1 *Formation and structural studies*

Figure 1 shows the TG/DTA curves obtained for gel precursor (intermediate compounds) of M = Al and M = Bi. The first weight loss regions from *RT*–220 °C (15% wt loss, figure 1a) and *RT*–165 °C (6% wt loss, figure 1(b) for M = Al and M = Bi due to loss of adsorbed water molecules. The second weight loss regions from 220 to 310 °C (31% wt loss, figure 1a) and 165–300 °C (51% wt loss, figure 1b) for M = Al and M = Bi is due to the loss of crystalline water molecules. The third weight loss regions from 310 to 460 °C (46% wt loss, figure 1a) and 300–465 °C (27% wt loss, figure 1b) for M = Al and M = Bi is attributed to the decomposition of hydroxides and acetates leading to the formation of final product with CO_2 and H_2O as byproducts. The weight loss in each stage is in good agreement with the expected values. Based on TG data, the formation temperature is about 460 °C for both the compositions. Nevertheless, we have heated the intermediate compound up to 900 °C to ensure the formation of single phase $LiNi_{0.4}M_{0.1}Mn_{1.5}O_4$ (M = Al, Bi) compounds.

XRD pattern of $LiNi_{0.4}M_{0.1}Mn_{1.5}O_4$ (M = Al, Bi) (figure 2) confirms the well-crystallized cubic spinel structure with *Fd3m* space group (JCPDS file no. 89–8325). Assuming that the XRD peak broadening depends only on crystallites size, the average crystallites size d was calculated using Scherrer's formula:

$$d = K\lambda/\beta\cos\theta,$$

where K is the shape factor (0·9–1·1), λ the incident X-ray wavelength (CuKα = 1·542 Å), β the full width half maximum in radians of the prominent line, i.e. (111) and θ-position of that line in the pattern. The d value is about 80 nm for M = Al and 100 nm for M = Bi.

The local environment of the cations in a cubic close packed oxygen array of the $LiNi_{0.4}M_{0.1}Mn_{1.5}O_4$ (M = Al, Bi) lattice were investigated by using FT–IR spectroscopy. The spectral high frequency bands have been observed at 500 and 620 cm^{-1} (figure 3a) for M = Al and at 500 and 600 cm^{-1} (figure 3b) for M = Bi. The band around 500 cm^{-1} has been assigned to Li–O stretching vibration, which indicates the formation of LiO_6 octahedra. The bands around 620 and 600 cm^{-1} are assigned to Li–Mn–O stretching vibrations which indicates the formation of MnO_6 octahedra (Helan and Berchmans 2011). These values are similar to the reports of Yi *et al* (2006) and Thirunakaran *et al* (2011).

SEM image of $LiNi_{0.4}M_{0.1}Mn_{1.5}O_4$ (M = Al, Bi) in figure 4 shows the polydispersed nature of particles and their agglomeration. The EDXA analysis shows the constituent elements (except Li which cannot be detected by EDXA) present in the expected levels as shown in the inset table.

Cation distribution and electronic structure of Mn^{4+} in the transition metal layers can be investigated by EPR spectroscopy, which has been used to obtain information of sample prepared. Changes in the manganese environment during lithium extraction/insertion can also be monitored by EPR spectroscopy.

$LiNi_{0.4}M_{0.1}Mn_{1.5}O_4$ (M = Al, Bi) contains two magnetic ions, Ni^{2+} (S = 2), Mn^{3+} (S = 2) and Mn^{4+} (S = 1/2). Ni^{2+}

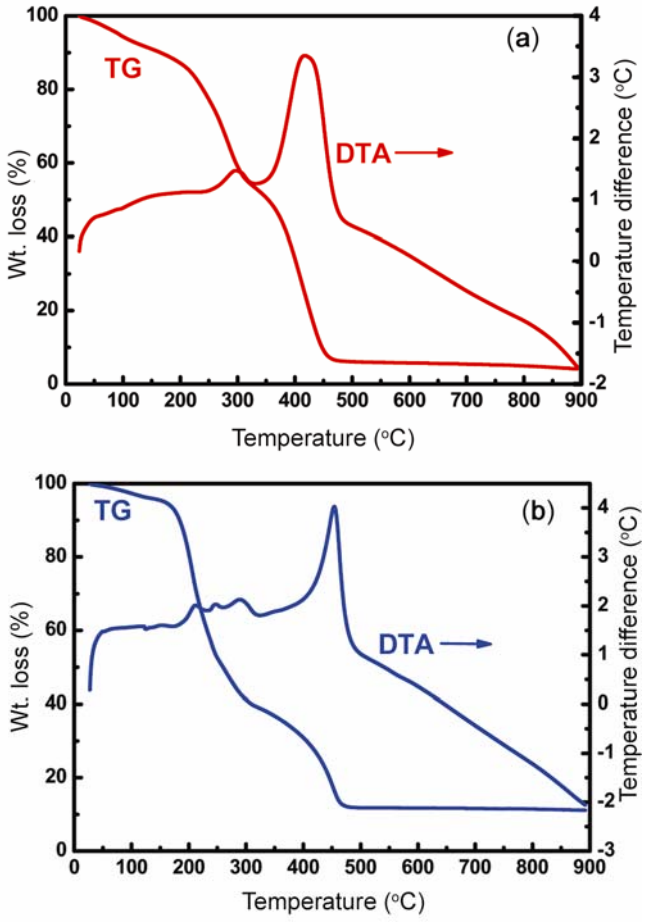

Figure 1. TG–DTA curves of intermediate precursors used to prepare $LiNi_{0.4}M_{0.1}Mn_{1.5}O_4$ where M = Al (**a**) and M = Bi (**b**).

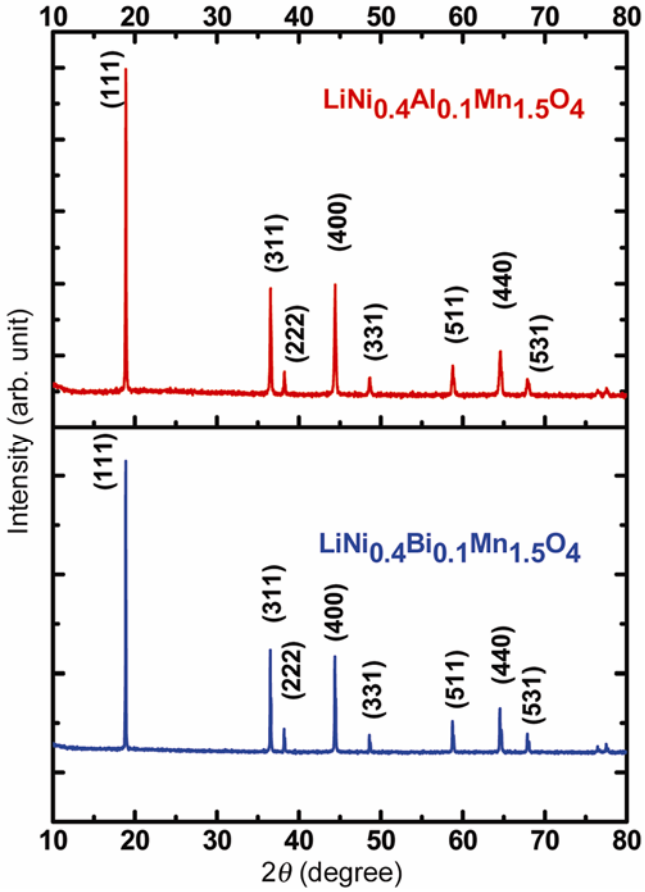

Figure 2. Powder XRD pattern of samples calcined at 900 °C.

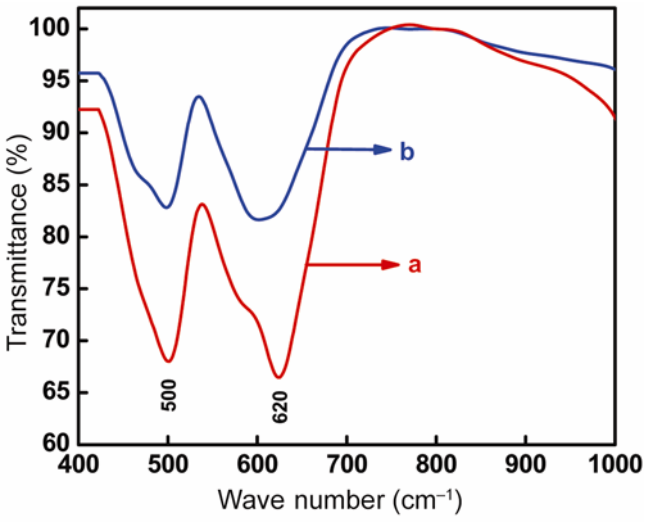

Figure 3. FT–IR spectra of $LiNi_{0.4}M_{0.1}Mn_{1.5}O_4$, where M = Al (a) and M = Bi (b).

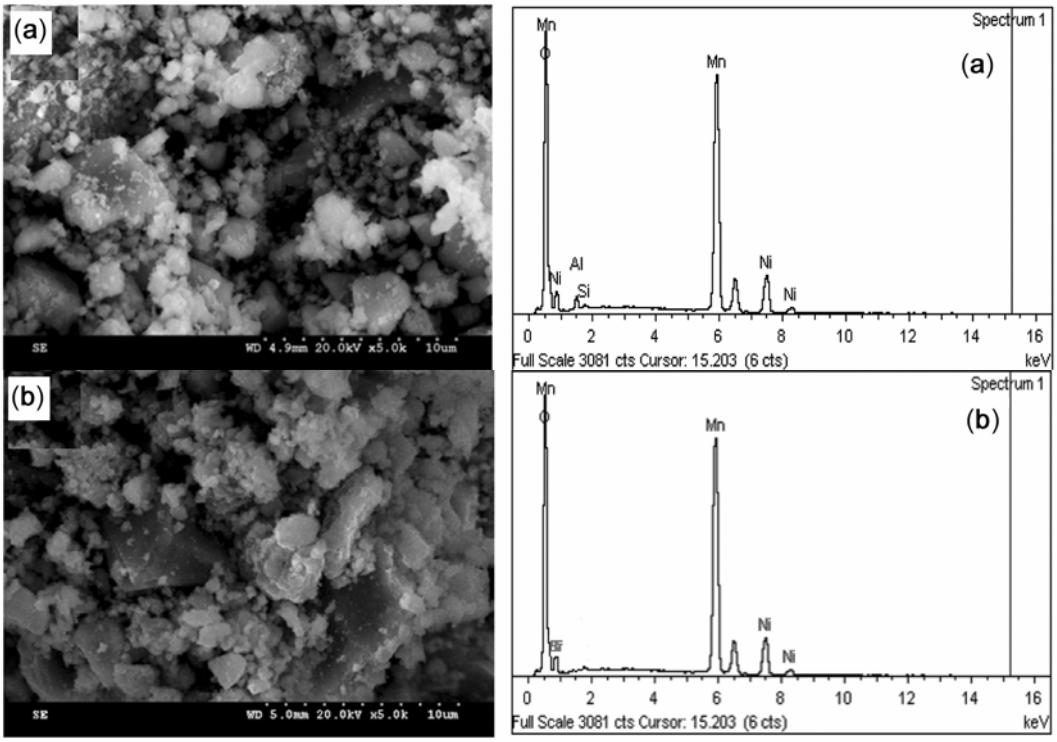

Figure 4. SEM image and EDAX spectra of $LiNi_{0.4}M_{0.1}Mn_{1.5}O_4$, where M = Al (**a**) and M = Bi (**b**).

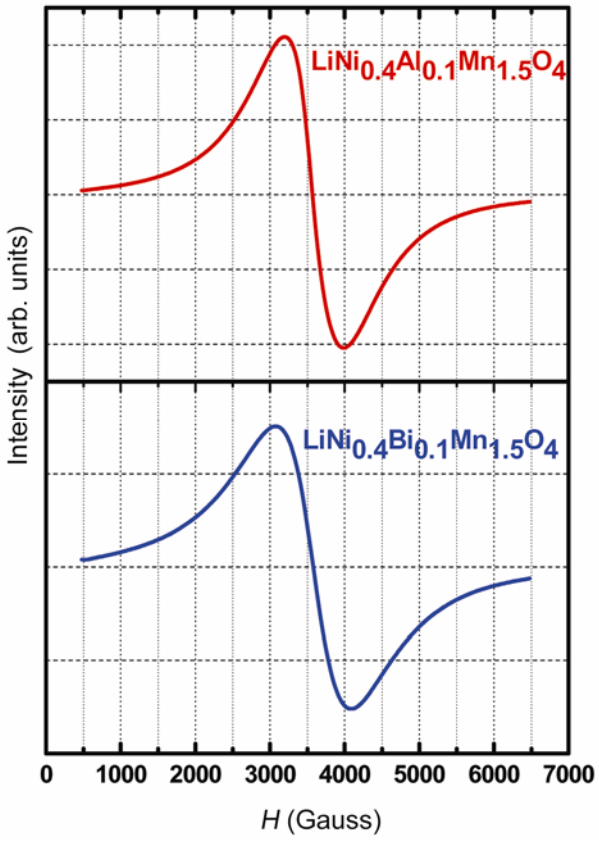

Figure 5. EPR spectra of samples calcined at 900 °C.

does not contribute to the EPR spectrum because the distortion of crystal field and strains on the different sites spreads out the resonance spectra and can no longer be detected. The detected paramagnetic resonance could only be attributed to the presence of octahedral Mn^{4+} ions that carry a half-integer spin (S = 3/2) and are then EPR-active. EPR spectra recorded for as prepared samples are shown in figure 5. The broad signal with Lorentzian shape centered at $g \approx 1{\cdot}74$ dominates in the EPR spectra. It is an indicative of the ordered nature of the sample having paramagnetic interaction between Mn^{3+} (S = 2) and Mn^{4+} (S = 3/2) ions in the spinel structure (Massarotti *et al* 1997; Stoyanova *et al* 2000a). In the case of Li_2MnO_3, which contain Mn^{4+} alone, the EPR signal consists of a narrow Lorentzian line with $g \approx 1{\cdot}99$ due to the magnetic coupled Mn^{4+} in ($LiMn_2$) layers (Massarotti *et al* 1997; Stoyanova *et al* 2000b).

3.2 *Electrical and electrochemical studies*

In order to study the kinetics of lithium insertion/exertion process, Nyquist plots of the $LiNi_{0.4}M_{0.1}Mn_{1.5}O_4$ (M = Al, Bi) is recorded, figure 6. An equivalent circuit describing the Randles model is used for fitting the experimental data (inset of figure 6) where R_s is the ohmic resistance, R_t is the charge transfer resistance of the electrodes, Z_w is the Warburg impedance and Q_c is the constant phase element. Constant phase element has been used to

accommodate capacitor imperfections. The calculated value fitted well with the experimental values. A high frequency semicircle and a sloping line in the low frequency region are obtained. The former represents the migration of the Li^+ ions at the electrode/electrolyte interface, whereas the low frequency range corresponds to the charge-transfer process (Takahashi *et al* 2002). The broad phase-transition peaks here indicate that the sample particles are not highly oriented (Aurbach *et al* 1998). The charge-transfer resistance is found to be about 440 Ω (figure 6a) for M = Al and 230 Ω (figure 6b) for M = Bi. These values indicate the formation of electrode/electrolyte interface layer on the surface of cathode after charge–discharge cycling. This observation is in corroboration with the previous reports (Shenouda and Murali 2008; Katiyar *et al* 2009).

Cyclic voltammograms were recorded with a CR-2032 coin type cells having $LiNi_{0·4}M_{0·1}Mn_{1·5}O_4$ (M = Al, Bi)/$LiPF_6$ + (EC + DMC)/Li at room temperature with a scan rate of 0·1 mV s^{-1}. Figure 7 shows the reversibility redox behaviour of $Mn^{3+/4+}$ upon deintercalation/intercalation of Li^+ ions over the voltage range of 3·5–4·9 V vs Li/Li^+. The redox behaviour observed here is in agreement with previous reports (ca. Tarascan and Guyomard 1991). The lithium removal (charge)-lithium uptake (discharge) in to the spinel structure involves one lithium equivalent per mole with an associated theoretical capacity of the material (Hassoun *et al* 2011). As shown in figure 7(a and b), there are two pairs of redox current peaks, viz. 3·95/4·07 V and 4·59/4·8 V for M = Al and 3·8/3·9 V and 4·4/4·8 V for M = Bi. These two pairs of redox peaks correspond to a two-step reversible intercalation process wherein Li-ions occupy two different tetragonal 8a sites in spinel $Li_xMn_2O_4$ ($x < 1$) lattice (Aklalouch *et al* 2009; Hassoun *et al* 2011). Deintercalation of Li^+ ions at higher potential indicates that more

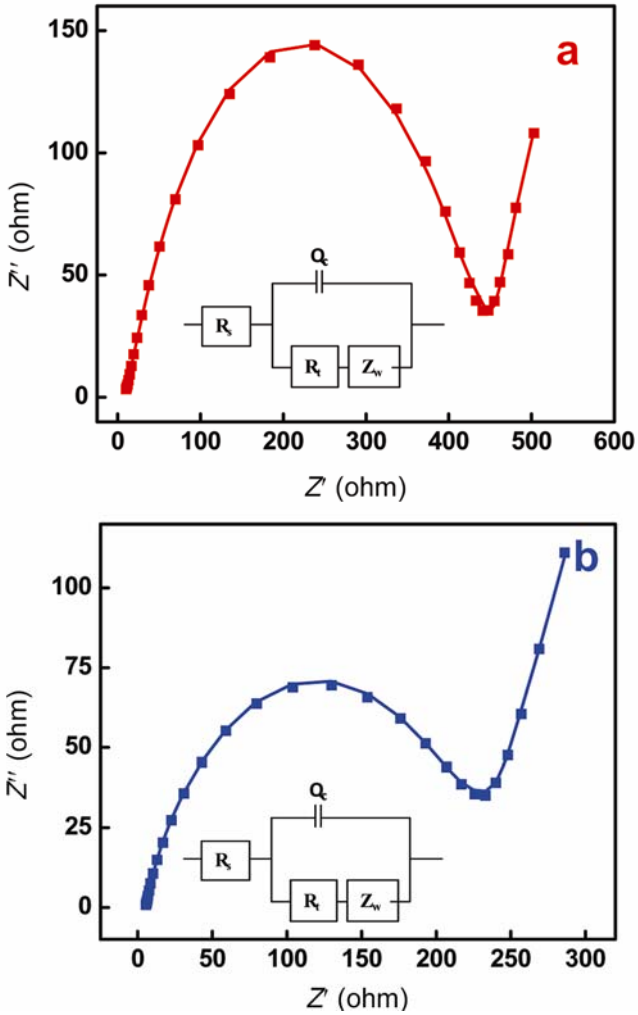

Figure 6. Nyquist plots of $LiNi_{0·4}M_{0·1}Mn_{1·5}O_4$, where M = Al (**a**) and M = Bi (**b**)/half cell fitted to Randles equivalent circuit.

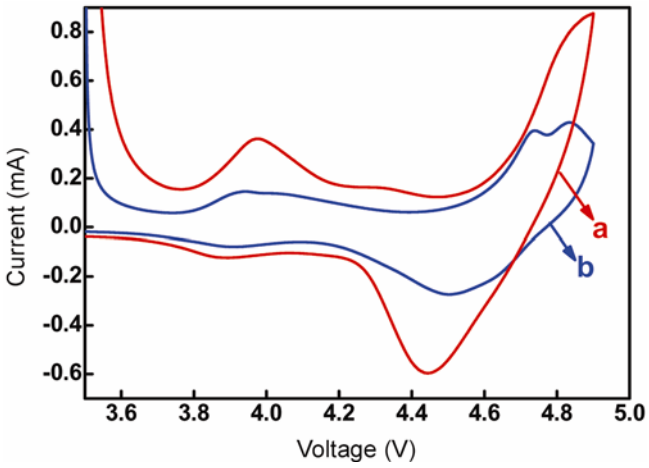

Figure 7. Cyclic voltammogram of $LiNi_{0·4}M_{0·1}Mn_{1·5}O_4$, where M = Al (a) and M = Bi (b) at scan rate of 0·1 mV s^{-1}.

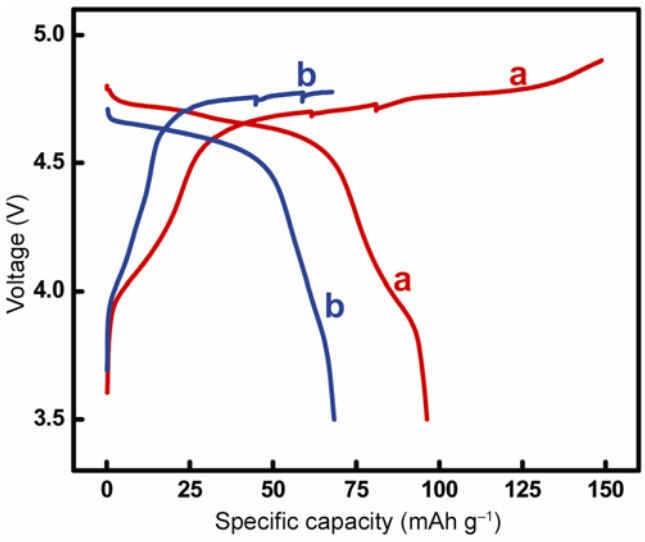

Figure 8. Galvanostatic voltage with specific capacity profiles for $LiNi_{0·4}M_{0·1}Mn_{1·5}O_4$, where M = Al (a) and M = Bi (b).

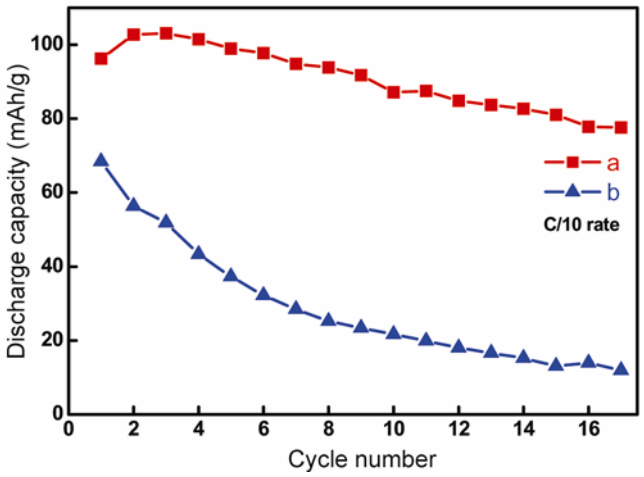

Figure 9. Variation of specific discharge capacity with cycle number for $LiNi_{0.4}M_{0.1}Mn_{1.5}O_4$, where M = Al (a) and M = Bi (b).

driving force is necessary to impel the Li-ions from the host structure to the anode.

Figure 8 shows the galvanostatic charge/discharge curves at a constant current rate of C/10 between 3·5 and 4·9 V. Figure 9 depicts the cycling performance of the $LiNi_{0.4}M_{0.1}Mn_{1.5}O_4$ (M = Al, Bi) electrode over 17 cycles. It can be seen that the initial discharge capacity was 96 and 68 mAh g^{-1} for M = Al and M = Bi, while at the end of 17 cycles, it was decreased to 77 and 11 mAh g^{-1}, respectively. It is important to note that, for M = Bi, we see relatively large discharge capacity when compared to M = Al. Thus, Al-doped sample is better than that of Bi-doped sample. In general, the specific capacity decreases at high current rates may be attributed to an increase of electrode polarization during cycling (Nithya *et al* 2011). In addition to hindered redox process of the cathode material, the electrode polarization can arise due to its incompatibility with current collector and also the electrolyte (Linden 1995). The reason for capacity fading has been attributed to many reasons as mentioned in the introduction part here. In the present case, the capacity fading is more pronounced in the case of Bi-doped sample. We think this is due to the relatively less stable lattice structure as the ionic radius of Bi^{3+} (1·2 Å) is much bigger than that of Mn^{3+} (0·65 Å) ≈ Al^{3+} (0·57 Å). Such a difference in ionic size will impose lattice distortion and instability on the solid solutions.

4. Conclusions

$LiNi_{0.4}M_{0.1}Mn_{1.5}O_4$ (M = Al, Bi) material in the powder form was successfully prepared by citric acid assisted sol–gel method and characterized by XRD, FT–IR, SEM and TG/DTA. Cyclic voltammogram for these material using CR-2032 coin-type cell shows two pairs of redox peaks at about 3·95/4·07 V and 4·59/4·8 V vs Li for M = Al and 3·8/3·9 V and 4·4/4·8 V vs Li for M = Bi. These values correspond to a two-step reversible intercalation reaction. Li-ion migration through the interface, i.e. from the surface layer of the particles to the electrolyte, is indicated from the high frequency semicircle followed by a sloping line in the low frequency region. The galvanostatic charge/discharge curves for M = Al (77 mAh g^{-1}) showed reasonably good capacity retention than that of M = Bi (11 mAh g^{-1}) at the end of 17 cycles. It is of interest to focus on the Al-doped sample for further investigation to enhance the capacity retention over large number of cycles.

Acknowledgements

We thank Dr T Premkumar of CECRI, Karaikudi, for providing experimental facility and Dr Harish C Barshilia of NAL, Bangalore, for SEM/EDX data.

References

Aklalouch M, Rojas R M, Rojo J M, Saadaune I and Amarilla J M 2009 *Electrochim. Acta* **54** 7542

Amarilla J M, Petrov K, Picó F, Avdeev G, Rojo J M and Rojas R M 2009 *J. Power Sources* **191** 591

Amatucci G, Pasquier A D, Blyr A, Zheng T and Tarscon J M 1999 *Electrochim. Acta* **45** 255

Aurbach D, Levi M D, Levi E, Telier H, Markovsky B and Salitra G 1998 *J. Electrochem. Soc* **145** 3024

Hassoun J, Lee K S, Sun Y K and Scrosati B 2011 *J. Am. Chem. Soc.* **133** 3139

Helan M and Berchmans L J 2011 *Mater. Manuf. Proc.* **26** 1369

Huggins R A 2008 *Advanced batteries – materials science aspects* (Stanford: Stanford University)

Katiyar R K, Singhal R, Asmar K, Valentin R and Katiyar R S 2009 *J. Power Sources* **194** 526

Ke D, Rong H G, Dong P Z and Lu Q 2010 *Electrochim. Acta* **55** 1733

Kim J and Manthiram A 1997 *Nature* **390** 265

Linden D 1995 *Handbook of batteries* (New York: McGraw-Hill)

Massarotti V, Capsoni D, Bini M, Azzoni C B and Paleari A 1997 *J. Solid State Chem.* **128** 80

Michalska M, Lipińska L, Mirkowska M, Aksienionek M, Diduszko R and Wasiucionek M 2011 *Solid State Ionics* **188** 160

Nithya C, Thirunakaran R, Sivashanmugam A and Gopukumar S 2011 *J. Power Sources* **196** 6788

Okubo M, Hosono E, Kim J, Enomoto M, Kojima N, Kudo T, Zhou H and Honma I 2007 *J. Am. Chem. Soc.* **129** 7444

Poizot P, Laruelle S, Grugeon S, Dupont L and Tarascon J M 2000 *Nature* **407** 496

Shenouda A Y and Murali K R 2008 *J. Power Sources* **176** 332

Shin Y and Manthiram A 2002 *Electrochem. Solid State Lett.* **5** A55

Shin Y and Manthiram A 2003 *Chem. Mater.* **15** 2954
Stoyanova R K, Zhecheva E N and Gorova M Y 2000a *J. Mater. Chem.* **10** 1377
Stoyanova R, Gorova M and Zhecheva E N 2000b *J. Phys. Chem. Solids* **61** 615
Takahashi M, Tobishima S I, Takei K and Sakurai Y 2002 *Solid State Ionics* **148** 283
Tarascan J M and Guyomard D 1991 *J. Electrochem. Soc.* **138** 2864
Thirunakaran R, Ravikumar R, Vanitha S, Gopukumar S and Sivashanmugam A 2011 *Electrochim. Acta* **58** 348
Wang G X, Bradhurst D H, Liu H K and Dou S X 1999 *Solid State Ionics* **120** 95
Whitfield P S and Davidson I J 2000 *J. Electrochem. Soc.* **147** 4476
Ye T S H, Bo J K, Li C Z, Cao J S, Sun Q L and Wang Y L 2010 *Electrochim. Acta* **55** 2972
Yi T, Hu X and Gao K 2006 *J. Power Sources* **162** 636